AD-A143 329 ANALYSIS OF DYNAMIC MIXED-MODE CRACK TIP STRESS PATTERNS(U) WASHINGTON UNIV SEATTLE DEPT OF MECHANICAL ENGINEERING M RAMULU ET AL. MAY 84 UWA/DME/TR-84/49 1/1

UNCLASSIFIED N00014-76-C-0060 F/G 20/11 NL

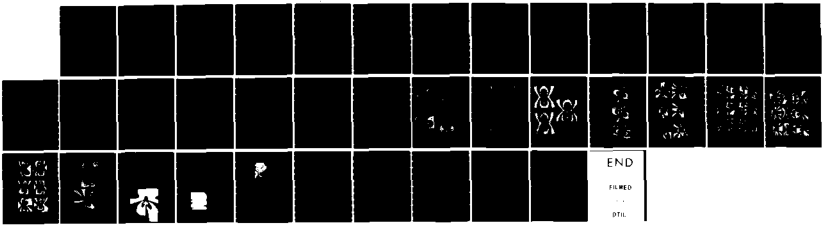

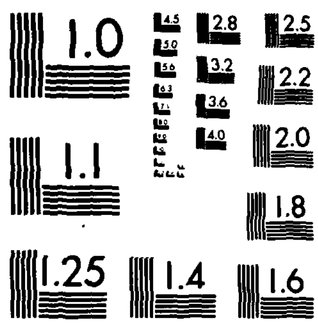

MICROCOPY RESOLUTION TEST CHART
NATIONAL BUREAU OF STANDARDS-1963-A

AD-A143 329

Office of Naval Research

Contract N00014-76-0060 NR 064-478

Technical Report No. UWA/DME/TR-84/49

ANALYSIS OF DYNAMIC MIXED-MODE CRACK TIP STRESS PATTERNS

by

M. Ramulu, D. B. Barker, and A. S. Kobayashi

May 1984

The research reported in this technical report was made possible through support extended to the Department of Mechanical Engineering, University of Washington, by the Office of Naval Research under Contract N00014-76-C-0060 NR 064-478. Reproduction in whole or in part is permitted for any purpose of the United States Government.

Department of Mechanical Engineering

College of Engineering

University of Washington

84 07 23 142

ANALYSIS OF DYNAMIC MIXED-MODE CRACK TIP STRESS PATTERNS

M. Ramulu*
D.B. Barker**
A.S. Kobayashi*

A1

ABSTRACT

The mixed-mode, elasto-dynamic state of stresses in the neighborhood of a rapidly running crack tip has been used to develop a relation between the isochromatic fringe order, N, and its position parameters, r and θ. The maximum shear stress is expressed in terms of the stress intensity factors K_I, K_{II}, σ_{ox} and other higher order terms involving the mixed-mode loading for a crack propagating at constant velocity. A graphics package based on these derivation was developed for mapping the isochromatics in the vicinity of a running crack tip and was used to illustrate typical mixed-mode isochromatics. The unsymmetry associated with higher order terms of mixed-mode stress field with the mode I singular stress field and with/without the mode II singular stress field also is investigated. Error estimates due to the assumed presence of K_{II} in a K_I stress field was found to be significant when the distance from the crack tip is more than 4mm.

* University of Washington, Department of Mechanical Engineering, Seattle, Washington 98195

** University of Maryland, Department of Mechanical Engineering, College Park, Maryland 20742

INTRODUCTION

While much has been discussed theoretically and experimentally on mixed-mode crack propagation [1-4], all discussions involved only quasi-static mixed-mode crack propagation. As for rapidly propagating cracks, there exists ample experimental evidence which shows that dynamic effects significantly affect the crack tip stress fields [5-10]. Dynamic analysis of a rapidly propagating crack is also required for interpreting the observed crack curving and crack bifurcations in brittle materials. The directional stability of a rapidly running crack has been shown to be influenced by crack velocity and the non-singular stress, σ_{ox}, which is the second order term in the crack-tip stress field. This stability problem was discussed theoretically and verified experimentally with dynamic photoelastic results by the authors [11,12] and Rossmanith [13]. These photoelastic results are based on data measurements in the vicinity of the crack tip and can introduce errors in estimated values of fracture parameters due to crack tip blunting, insufficient fringe resolution and inaccurate determination of crack tip location. On the other hand, other far field errors may be introduced when data away from this crack tip zone together with higher order terms in the crack tip stress field is used to characterize the near crack tip stress field.

Two and three parameter characterization of static and dynamic stress fields under pure mode I loading condition has been studied exhaustively by Rossmanith and Irwin [7]. The effects of the first higher order term, σ_{ox}, which is the lowest order non-singular term and represents the stress biaxiality at the crack tip, were studied by Kobayashi and Ramulu [9-12] for static and dynamic mixed-mode conditions. In a recent investigation, Rossmanith [14] observed that the unsymmetry of isochromatics can be generated by superimposing higher order terms of mode II stresses on mode I stress field

away from the crack tip. Our dynamic photoelastic analyses of crack curving and crack branching experiments, however, showed that the unsymmetry of isochromatics at a distance as close as 1 to 3mm from the crack tip was always associated with dynamic K_{II} and hence with directionally unstable cracks. Because the relative magnitude of such dynamic K_{II} is small with respect to the dominating dynamic K_I values for many crack propagation problems and its influence on the far field isochromatics is usually small. On the other hand, unsymmetry in the far field isochromatics may not require the presence of dynamic K_{II}, as reported by Rossmanith [14] and thus, error estimates in the fracture parameters due to the assumed presence of K_{II} in a K_I stress field is needed. A numerical experimentation based on the theoretical dynamic isochromatic field could provide not only the errors involved in wrongful presence of dynamic K_{II}, but also could provide information the minimum number of higher order terms needed in the crack tip stress field and region of influence of the near crack tip field under dynamic conditions for accurate assessment of the dynamic crack tip stress field.

The objective of the present investigation is to study the effects of higher order terms on the mixed-mode crack tip stress pattern of a rapidly running crack with an attempt to rationally delineate the optimum region of data collection. The effects of higher crack velocity on the crack tip stress pattern which has not been reported previously under mixed-mode loading also are presented.

THEORY

The general near crack tip dynamic state of stresses under mixed-mode conditions was given recently by Nishioka and Atluri [15] in terms of the local rectangular (x,y) and polar (r,θ) coordinates. The three rectangular stress components under mode I and mode II conditions are given as

$$
\begin{bmatrix} \sigma_{xx} \\ \sigma_{yy} \\ \sigma_{xy} \end{bmatrix} = \sum_{n=1}^{\infty} A_{In} \frac{B_1(c)}{\sqrt{2\pi}} \frac{n(n+1)}{2} \begin{bmatrix} (1+2S_1^2-S_2^2) r_1^{(\frac{n}{2}-1)} \cos(\frac{n}{2}-1)\theta_1 - 2h(n) r_2^{(\frac{n}{2}-1)} \cos(\frac{n}{2}-1)\theta_2 \\ -(1+S_2^2) r_1^{(\frac{n}{2}-1)} \cos(\frac{n}{2}-1)\theta_1 + 2h(n) r_2^{(\frac{n}{2}-1)} \cos(\frac{n}{2}-1)\theta_2 \\ -2S_1 r_1^{(\frac{n}{2}-1)} \sin(\frac{n}{2}-1)\theta_1 + \frac{(1+S_2^2)}{S_2} h(n) r_2^{(\frac{n}{2}-1)} \sin(\frac{n}{2}-1)\theta_2 \end{bmatrix}
$$

$$
+ \sum_{n=1}^{\infty} A_{IIn} \frac{B_{II}(c)}{\sqrt{2\pi}} \frac{n(n+1)}{2} \begin{bmatrix} (1+2S_1^2-S_2^2) r_1^{(\frac{n}{2}-1)} \sin(\frac{n}{2}-1)\theta_1 - 2h(\bar{n}) r_2^{(\frac{n}{2}-1)} \sin(\frac{n}{2}-1)\theta_2 \\ -(1+S_2^2) r_1^{(\frac{n}{2}-1)} \sin(\frac{n}{2}-1)\theta_1 + 2h(\bar{n}) r_2^{(\frac{n}{2}-1)} \sin(\frac{n}{2}-1)\theta_2 \\ 2S_1 r_1^{(\frac{n}{2}-1)} \cos(\frac{n}{2}-1)\theta_1 - \frac{(1+S_2^2)}{S_2} h(\bar{n}) r_2^{(\frac{n}{2}-1)} \cos(\frac{n}{2}-1)\theta_2 \end{bmatrix} \quad (1)
$$

where

$$
S_1^2 = 1 - \frac{C^2}{C_1^2} \quad ; \quad S_2^2 = 1 - \frac{C^2}{C_2^2}
$$

$$
B_1(c) = \frac{1+S_2^2}{D(C)} \quad ; \quad B_{II}(c) = \frac{2S_2}{D(C)}
$$

$$
D(c) = 4S_1S_2 - (1+S_2^2)^2
$$

$$h(n) = \begin{cases} \dfrac{2S_1S_2}{1+S_2^2} : & n \text{ odd} \\ \dfrac{1+S_2^2}{2} : & n \text{ even} \end{cases} \qquad r_1^2 = x^2 + S_1^2 y^2 \qquad \operatorname{Tan}\theta_1 = S_1 \operatorname{Tan}\theta$$

$$r_2^2 = x^2 + S_2^2 y^2 \qquad \operatorname{Tan}\theta_2 = S_2 \operatorname{Tan}\theta$$

$$\operatorname{Tan}\theta = y/x$$

$$h(\overline{n}) = h(n+1) \qquad r^2 = x^2 + y^2$$

r and θ are the polar coordinates with origin at the moving crack tip and C, C_1, and C_2 are the crack velocity, dilatational and distortional wave velocities, respectively.

The general solution expressed in Equation (1) yields the singular stresses when n = 1; i.e., $A_{I1} = K_I$ and $A_{II1} = K_{II}$, which are stress intensity factors of mode I and mode II, respectively. The constant stress, σ_{ox}, is related to the higher order terms (HOT) for $n \geq 2$ as

$$\sigma_{ox} = \frac{-6\, B_I(c)(S_2^2 - S_1^2)}{\sqrt{2\pi}} A_{I2} \qquad (2)$$

$$A_{II2} = 0$$

The n = 2 term exists only in σ_{xx}, stress component of mode I loading and is zero in all other components of mode I and mode II stress fields. The influence of these and third order terms, n = 3, on the shape of the isochromatics surrounding the crack tip, are studied.

The analyses of mixed-mode isochromatics is made by computing the maximum shear stress contours around the crack tip. The maximum, in-plane shear stress, τ_m, is related to the cartesian stress components as

$$(2\tau_m)^2 = (\sigma_{yy} - \sigma_{xx})^2 + 2\,\tau_{xy}^2 \qquad (3)$$

The analytical expression for mixed-mode isochromatics in the vicinity of the

crack tip is obtained by combining the maximum shear stress, τ_m, and the stress optic law.

$$\tau_m = \frac{Nf_\sigma}{2h} \tag{4}$$

where N is the fringe order, f_σ is the stress-optical constant, and h is the specimen thickness. The combination of Equations (1-4) yields a highly complex relation which can be written in a functional form as

$$N = F(f_\sigma, h, r, K_I, K_{II}, \sigma_{ox}, C, C_1, C_2, \theta, HOT) \tag{5}$$

The isochromatic field near the crack tip for given fracture parameters of K_I, K_{II}, σ_{ox}, and the model parameters of f_σ and h as well as the crack velocity, C, may be generated by computing N at a large number of special points. Equation (5) is programmed to plot the dynamic isochromatics where the computer routine involved is similar to that discussed in References [3] and [9]. The τ_m values were computed for an array of points within a region of ± 25mm with the crack tip in the center.

NEAR CRACK TIP ISOCHROMATICS

As an accuracy check of Equation (5), the dynamic isochromatics should coincide with that of References [3] and [9] for the limiting case of crack velocity C -> 0 as well as $C = 0.15C_1$, respectively, for identical values of K_I, K_{II}, and σ_{ox}. These fracture parameters K_I, K_{II}, σ_{ox} and the other higher order terms through the third order were varied and crack tip isochromatic fringes were constructed. The size, shape, and orientation of these fringe patterns depend strongly on the combination of parameters chosen [3,4,9]. In order to visualize the effects of the higher order terms, theoretical isochromatics were generated using the same model-fringe constant of f_σ/h = 1.73 MPa/fringe (250psi/fringe), K_I = 0.876 MPa $\sqrt{m}$ (800psi $\sqrt{in}$) and K_{II} of

Reference [3]. A constant crack velocity of $C = 0.20C_1$; and $0.30C_1$ was chosen to generate the dynamic isochromatics. In addition, $C_1 = 2,400$m/s (94,300 in/s) and $C_2 = 1,160$ m/s (45,800 in/s), $K_{II}/K_I > 0$ were assumed in the dynamic analysis. Static isochromatics were generated by setting $C = 0.01\ C_1$ in Equation (5) and these plots were in agreement with that of References [3] and [4].

The static and dynamic isochromatics listed in Figures 1 through 8 can be broadly classified as:

a) Mode I ($A_{In} > 0 = 0$, $A_{II\,n} = 0$)

b) Mode II ($A_{In} = 0$, $A_{IIn} \neq 0$)

c) Mixed Mode ($A_{II1}/A_{I1} = K_{II}/K_I = 0.25$ and $A_{In} = A_{IIn} > 0$ when $n \geq 2$)

The higher order terms $A_{I2} \neq 0$ accounts for the stress biaxiality under mode I loading condition and is independent of the radial distance and the angle. The A_{I3} *and* A_{II3} *terms represents the influence of the near boundaries* on the isochromatics and its magnitude and sign depends on the loading configuration [4]. In the following discussion, some representative static and dynamic isochromatics in the vicinity of the crack tip are shown in Figure 1-8 for mode I, II, and mixed-mode loadings.

PURE MODE I ($A_{In} \neq 0$; $A_{IIn} = 0$ for $n \geq 2$)

The analytically generated pure mode I crack tip stress patterns with the effect of higher order terms of $n \geq 2,3$, which corresponds to r^0 and $r^{1/2}$, respectively, for a crack velocity of $C/C_1 = 0.2$, is shown in Figure 1. The fringe pattern tilt forward for $A_{I2} < 0$ and backwards for $A_{I2} > 0$. The added third order term of $A_{I3} < 0$ increases the maximum apogee distance r_{max} of the isochromatic for $A_{I2} < 0$ and decreases r_{max} when $A_{I2} > 0$. The effect of A_{I3} term is noted as the distance from the crack tip increases and appears to be an

essential term in the evaluation of fracture parameters using far-field data. Detailed discussion of mode I isochromatics can be found in Reference [7] and [9].

PURE MODE II (A_{In} = 0; $A_{IIn} \gtrless 0$ for n > 2)

Figure 2 shows the pure mode II static isochromatic stress field for $A_{II1} \neq 0$ and $A_{II3} > 0$. The effect of A_{II3} term is significant. When $A_{II1} > 0$ and $A_{II3} = 0$, the isochromatics are symmetric with respect to x and y. When A_{II3} is added to the pure mode II singular stress field, only the x axis symmetry is maintained.

Figure 3 shows the pure mode II singular crack tip stress patterns (n = 1) with increasing crack velocity C/C_1. As the crack velocity increases, the size of the isochromatics ahead of the crack tip decreases. Although there is no experimental evidence of a crack propagating rapidly under pure mode II loading, this numerical experiment demonstrates that the crack velocity significantly affects the isochromatic patterns.

MIXED MODE ($A_{In} > 0$, $A_{IIn} \neq 0$)

Superposition of a slight shearing stress component with and without the singular stress component destroys the symmetry of the mode I isochromatic pattern [14]. The mixed-mode cases are classified into three groups:

a) Mixed-mode with dominant mode I and higher order terms.

b) Mixed-mode with dominant mode II and higher order terms.

c) Unsymmetric isochromatics associated with higher orders of mode II terms in (a) and with higher orders of mode I terms in (b).

In the following, some representative static and dynamic isochromatics are presented.

Mode I Dominant Loading

Figure 4 shows the pure mixed-mode static and dynamic singular stress patterns for $K_{II}/K_I = 0.25$. The fringe patterns shown are symmetric and the axis of symmetry rotated clockwise about 25 degrees for $K_{II}/K_I = 0.25$, as observed by Rossmanith [4]. For $K_{II}/K_I = 0.25$, the axis of symmetry rotates counterclockwise about 25 degrees. Furthermore, the isochromatic fringe pattern distorts at higher crack velocities by shortening and stretching of the upper loops and lower loops, respectively. For $C/C_1 = 0.30$, the upper fringe loops tilt counterclockwise while the lower fringe loops do not rotate any further.

Figure 5 shows the mixed-mode crack tip stress pattern with a dominant mode I stress field. The isochromatics increase in size for the positive higher order terms of A_{I2}, A_{I3}, and for crack velocities of $0.2C_1$ and $0.3C_1$. The upper loop again tilts counterclockwise and flattens as the magnitude of C/C_1 increases to 0.3, as shown in Figure 5a. Similar effects were noted for the experimentally observed crack velocities of $C/C_1 = 0.2$, with the addition of the negative higher order terms of A_{I2} and A_{I3}. Addition of the third higher order term, A_{I3}, regardless of the sign of the A_{I2} in the stress field, increased the fringe size. Velocity effect is significant at $C/C_1 = 0.30$ for added terms of $A_{I2} \gtrless 0$.

The influence of A_{I3} and A_{II3} terms, which represent the boundary influence on the isochromatics, is shown in Figure 5b under mixed-mode loading, with $A_{I2} = 0$. For the equal magnitudes of A_{I3} and A_{II3}, the fringe loop size increased significantly and exhibited severe unsymmetric stress patterns away from the crack tip. However, in the near vicinity of the crack tip, the fringe pattern shape and orientation is quite similar to the fringe patterns of Figure 4.

This demonstrates the fact higher order terms must be included in the stress field characterization when far-field fracture data are used.

Mode II Dominant Loading

The crack velocity not only affects the mixed-mode isochromatics for mode I dominant loading but also for mode II dominant loading. Figure 6 shows the theoretically generated isochromatics with increasing mode II loading representing mode II dominant isochromatics. Under K_{II} loading, the fringe loops do not terminate at the crack tip and the fringe patterns become increasingly dissimilar. Increases in mode II loading rotates the fringe pattern counterclockwise with changes in shape and size.

Details of the changes in the shapes of the static mixed-mode isochromatics are discussed in Reference [4] and, thus, will not be reproduced here. In essence, the corresponding dynamic isochromatics are found to be larger and essentially follow the general shape of the static isochromatics. Similar results are shown in Figures 1 through 9 for the experimentally observed crack $C/C_1 = 0.2$.

Usymmetric Isochromatics

Usymmetric isochromatic patterns can be generated by adding $A_{II3} \gtrless 0$, with and without $A_{I3} \gtrless 0$. However, significant change in isochromatic patterns are noted when the sign of the remote-stress component σ_{ox}, i.e., A_{I2}, is changed. As shown in Figure 5, the fringe loops in the angular range of 0 to 180° decrease in size for a positive σ_{ox} and mode II stress intensity factor. The higher order terms ($n \geq 3$) appear to have a negligible effect on the isochromatics in the vicinity of the crack tip. The loss of symmetry and the distortion of the isochromatics, however, become more pronounced when higher

order terms without singular term mixed-mode loading ($A_{In} \neq 0$; $K_{II} = 0$, $A_{IIn} \neq 0$) are added. The fringe loops ahead of crack tip also do not terminate at the crack tip.

Figure 7 shows the effect of the higher order terms of mode II isochromatics with the mode I stress field. When $A_{II3} > 0$ is superposed onto the mode I stress field with $K_I > 0$ and $K_{II} = 0$, the resulting isochromatic stress pattern loses its x- and y-axis symmetries for all A_{I2}. Increase in crack velocity distorts this isochromatic pattern. Similar changes also are seen in the case of Figure 8, when the higher order terms of mode I stress field with $K_I = 0$, $A_{I2} \lesseqgtr 0$, and $A_{I3} = A_{II3} \gtrless 0$ are superposed onto pure mode II singular stress field.

Slight unsymmetry in load are often observed experimentally and are modeled with $K_{II} = 0$, $A_{II3} < 0$ in the presence of σ_{ox}. Such loading is superposed onto the mode I crack shown in Figure 9a. A genuine mixed-mode crack tip isochromatics is modeled with $K_{II}/K_I = 0.10$ and is also shown in Figure 9b. Both isochromatics exhibit slight unsymmetry and their shapes, sizes, and orientation are influenced not only by the crack velocity, C/C_1, but also by the ratio of mixed-mode stress intensity factors.

DISCUSSIONS

Figures 1, 3, 5, and 6 show that the crack velocity affects the isochromatics associated with mode I, II, and mixed-mode loading, and also in mode II dominant loading. Increasing crack speed tends to reduce the directional stability, which is generated by compressive stress parallel to the crack, irrespective of the modes of deformation as noted in the recently proposed crack curving criteria [11]. The added higher order terms change the shape and size, which are governed by the sign of these terms, of the transient

isochromatics. Although mode II stress intensity factor is zero, i.e., $K_{II} = 0$, in Figure 9a, the presence of other higher order terms of the opening and shearing mode stress field generated unsymmetric isochromatics. Figure 9b shows only a slight unsymmetry observed in the presence of a smaller amount of K_{II}/K_I. Such unsymmetric isochromatics are typically associated with curved crack and post branching cracks.

In order to demonstrate the errors involved by assuming a mixed-mode crack tip stress field (K_I, K_{II}, and σ_{ox}), the grossly unsymmetric isochromatics of Figure 9a is chosen for a numerical experiment. This numerical experiment will provide assessments of the effective region of the crack-tip stress field and of the terms needed for obtaining accurate fracture parameters. By applying the overdeterministic procedure [9,16], the fracture parameters with added higher order terms were evaluated using the fringe orders 3, 4, and 5 in Figure 9a. A total of 20 data points which were located in the vicinity of the maximum radial distance from the crack tip in each fringe order were used. Data points were taken over the range $2mm < r_{max} < 8.5mm$, at several values of r. Table 1 shows the two-parameter (K_I, σ_{ox}), three-parameter (K_I, K_{II}, σ_{ox}), and five-parameter (A_{In}, A_{IIn} for n = 1,2,3), which were determined by this numerical experiment and the exact values associated with the theoretical isochromatics. These results show that the fracture parameters generated by this far-field data result in an apparent K_{II} in addition to K_I. This finding is in agreement with the results of Rossmanith [14], where K_{II} diminishes as the data points closer to the crack tip are used in data reduction. The estimated fracture parameters, which were obtained by using five-parameter, also overestimated the stress intensity factor. Again, this error decreased when the nearest fringe was used. These unsymmetric patterns in the absence of K_{II} are found to be present only when r is greater than about 4mm.

In the presence of a small mode II stress intensity factor, the analytically generated isochromatics exhibits unsymmetry at a radial distance as small as r = 1mm and is always associated with a kinked crack. Table 1 also shows that the five parameter method appears less desirable with added difficulty in numerical convergency. Also, the constant crack speed assumption is reasonable only if the measurement region is restricted to a moderate size as specified in Reference [17]. Finally, this numerical experimentation confirms the general validity of the three-parameter method.

Typical mixed-mode experimental and theoretical isochromatics are shown in Figures 10 through 12. The data points for generating the theoretical isochromatics were taken over a region of radius 1 to 4mm, centered at the crack tip. The theoretically generated isochromatics, with and without higher orders, matched the experimental fringe patterns within the sampled region around the crack tip.

Figure 10 shows one enlarged frame out of a 16-frame dynamic photoelastic record of a curved crack in a 9.5mm thick, 254 x 254mm Homalite-100 single-edge-notch (SEN) specimen loaded under fixed-gripped tension [11]. K_I, K_{II}, and σ_{ox} were estimated by the three-parameter method and is used to reconstruct the experimental isochromatics. The mixed-mode effect is visible for a radial distance as small as 1mm and the theoretical and experimental isochromatics agree reasonably well within the region of about 4mm. The isochromatics associated with the continuously curving post-branched crack in a wedge-loaded rectangular double cantelever beam (WL-RDCB) specimen [12] is shown in Figure 11. The noticeable unsymmetry is not due only to the higher order terms of mode II loading, but to the genuinely mixed-mode crack tip deformation of $K_{II}/K_I = -0.17$. The analytically generated isochromatics matched well with the experimental isochromatics within the sampled region.

Figure 12 shows the arrested branch crack with a dominant mode II crack tip deformation during unloading process in a 3.2mm thick, 127 × 225mm polycarbonate single-edge notch specimen [18]. The theoretical and experimental isochromatics matched better within a crack tip zone of 4mm when the three parameter method, without the higher order terms, was used for data reduction. Thus, fracture parameters associated with directionally stable and unstable cracks can be determined with reasonable accuracy by the three parameter method as long as the data points are within a circular region of radius 4mm from the crack tip.

Finally, the possible errors in crack curving angles which were generated by using the mixed-mode three parameter (K_I, K_{II}, σ_{ox}) characterization of unsymmetric isochromatics of K_I field, were estimated by using the fracture parameters generated by the nearest fringe order data in Table 1. The estimated fracture parameters with the nearest or highest fringe order from Table 1 yield an apparent mixed-mode stress intensity factor ratio of K_{II}/K_I = -0.026. By assuming a critical radius of r_c = 1.3mm [11,12], the parameter $\sqrt{r_c}\frac{\sigma_{ox}}{K_I}$, which controls the direction of crack propagation, becomes -0.0569. This data is used to predict the crack curving angles by using the maximum circumferential stress theory.

Figure 13 shows the influence of K_{II}/K_I on the analytically predicted crack kinking angles for $\sqrt{r_c}\frac{\sigma_{ox}}{K_I}$ = -0.05690, 0.0, and 0.0569. A mixed-mode stress intensity factor ratio of K_{II}/K_I = -0.0155 or -0.036 with a positive or negative $\sqrt{r_c}\frac{\sigma_{ox}}{K_I} = \pm 0.0569$, respectively, is required to generate a measurable crack curving angle of 3 degrees. Thus, in the presence of a negative $\sqrt{r_c}\frac{\sigma_{ox}}{K_I}$, the magnitude of K_{II}/K_I must double that required for a positive $\sqrt{r_c}\frac{\sigma_{ox}}{K_I}$ in order to generate a visible crack curving. On the other hand, a hypothetical K_{II} = -0.026 K_I with $\sqrt{r_c}\frac{\sigma_{ox}}{K_I}$ = -0.0569 will result in a crack kinking angle of

1.8 degrees, which is negligible. By changing $\sqrt{r_c}\,\frac{\sigma_{ox}}{K_I} = 0.0569$, the kinking angle increases to 4.2 degrees, which is noticeable. Such positive $\sqrt{r_c}\,\frac{\sigma_{ox}}{K_I}$, however, is only remotely possible. The predicted crack curving angle from the evaluated fracture data of the unsymmetric isochromatics is at the most 1.8 degrees and is barely noticeable. Possible errors which are generated by using three parameter method (K_I, K_{II}, σ_{ox}) in evaluating the unsymmetric isochromatics without a singular mode II is negligible if the photoelastic data is confined to a circular region of radius 4mm from the crack tip.

The above results address the question of the needed terms in the dynamic mixed-mode crack tip stress field, and also indicate the limitation in crack tip zone size for accurate estimation of stress intensity factors. In order to define the conditions under which the higher order terms need to be included in the dynamic stress field remains a topic worthy of detailed investigation.

CONCLUSIONS

1. The higher order terms significantly affect the size and shapes of dynamic crack-tip isochromatics generated by pure mode I, mode II, and under mixed-mode loadings. In particular, the first higher order term or remote stress component changes the crack tip stress pattern shape and size in all modes of loading.

2. The higher order terms of $n = 3$, i.e., A_{I3}, A_{II3}, significantly affect the isochromatics and must be used in analyzing the pure mode II fracture.

3. Crack velocity of $C/C_1 > 0.2$, alter significantly the size and shape of the crack tip stress pattern in all modes of loading.

4. The higher order terms ($n > 3$) have little influence on the elastodynamic mixed-mode isochromatics for a radial distance less than 4mm.

5. The isochromatics can become unsymmetric in the presence of higher order

terms in mode II stress field without the presence of the singular term involving K_{II}.

6. By using the three parameter model one can estimate reasonably accurate fracture parameters associated with directionally stable and unstable cracks within the maximum radial distance of 1 to 4mm.

ACKNOWLEDGEMENT

The work reported here was obtained under ONR Contract NO-0014-76-C-000 NR-064-478. The authors wish to acknowledge the support and encouragement of Y. Rajapakse, ONR, during the course of this investigation.

REFERENCES

1. Smith, D.G., and Smith, C.W., "Photoelastic Determination of Mixed Mode Stress Intensity Factors," Eng. Fract. Mech., 4, 357-366, 1972.

2. Gdoutos, E.E., and Theocaris, P.S., "A Photoelastic Determination of Mixed-Mode Stress-Intensity Factors," Exp. Mech., 18, 87-96, 1978.

3. Dally, J.W., and Sanford, R.J., "Classifications of Stress Intensity Factors from Isochromatic Fringe Patterns," Exp. Mech., 18, 441-448, 1978.

4. Rossmanith, H.P., "Analysis of Mixed-Mode Isochromatic Crack-Tip Fringe Patterns," Acta Mechanica, 34, 1-38, 1979.

5. Bradley, W.B., and Kobayashi, A.S., "Fracture Dynamics - A Photoelastic Investigation," Eng. Fract. Mech., 3, 317-332, 1971.

6. Dally, J.W., "Dynamic Photoelastic Studies of Fracture," Exp. Mech., 19, 349-367, 1979.

7. Rossmanith, H.P., and Irwin, G.R., "Analysis of Dynamic Isochromatic Crack-Tip Stress Patterns," University of Maryland Report, 1979.

8. Rossmanith, H.P., and Shukla, A., "Dynamic Photoelastic Investigation of Interaction of Stress Waves with Running Cracks," Exp. Mech., 21, 415-422, 1981.

9. Kobayashi, A.S., and Ramulu, M., "Dynamic Stress Intensity Factors for Unsymmetric Dynamic Isochromatics," Exp. Mech., 21, 41-48, 1981.

10. Kobayashi, A.S., and Ramulu, M., "Dynamic Mixed-Mode Fracture," Proc. US-Greece Symp. on Mixed-Mode Crack Propagation, ed. by G.C. Sih and P.S. Theocaris, Sijthoff & Noordhoff, 163-172, 1981.

11. Ramulu, M., and Kobayashi, A.S., "Dynamic Crack Curving - A Photoelastic Evaluation," Exp. Mech., 23, 1-9, 1983.

12. Ramulu, M., Kobayashi, A.S., and Kang, B. S-J., "Dynamic Crack Branching - A Photoelastic Evaluation," Fracture Mechanics (15), ASTM/STP, 1983, to be published.

13. Rossmanith, H.P., "Crack Propagation and Branching," Proc. Symp. on Absorbed Spec. Energy/Strain Energy Density, Eds. G.C. Sih, E. Czoboly, and F. Fillemot, Budapest, Hungary, 283-294, 1981.

14. Rossmanith, H.P., "How Mixed is Dynamic Mixed-Mode Crack Propagation? - A Dynamic Photoelastic Study," J. Mech. Phys. Solids, 31, 251-260, 1983.

15. Nishioka, T., and Atluri, S.N., "Path Independent Integrals, Energy Release Rates, and General Solutions of Near-Tip Fields in Mixed Mode Dynamic Fracture Mechanics," Eng. Fract. Mechanics., 17, 1-22, 1983.

16. Sanford, R.J., and Dally, J.W., "A General Method for Determining Mixed Mode Stress Intensity Factors from Isochromatic Fringe Patterns," Eng. Fract. Mech., 11, 621-633, 1979.

17. Rossmanith, H.P., and Chona, R., "A Survey of Recent Developments in the Evaluation of Stress Intensity Factors from Isochromatic Crack-Tip Stress Patterns," ICF V, Cannes, Vol. V, 2507-2516, 1981.

18. Ramulu, M., Kobayashi, A.S., Kang, B.S.J., and Barker, D.B., "Further Studies on Crack Branching," Exp. Mech., 23, 431-437, 1983.

TABLE 1

Evaluation of Fracture Parameters
Associated with the Fringe Pattens Shown in Figure 12a

		ESTIMATION								
	EXACT VALUES	TWO PARAMETER			THREE PARAMETER			FIVE PARAMETER		
FRINGE ORDER		3	4	5	3	4	5	3	4	5
K_I (MPa$\sqrt{m}$)	0.876	0.810	0.820	0.820	1.049	0.954	0.873	0.986	1.041	0.892
A_{I2} (MPa)	-0.58	-1.20	-0.78	-0.72	-0.73	-0.50	-0.59	-0.83	-0.37	-0.62
A_{I3} (MPa/$\sqrt{m}$)	0	--	--	--	--	--	--	-0.69	-0.17	-0.35
K_{II} (MPa$\sqrt{m}$)	0	--	--	--	-0.043	-0.023	-0.019	0.077	-0.043	-0.022
A_{II3} (MPa/$\sqrt{m}$)	-0.28	--	--	--	--	--	--	0.35	0.30	-0.35

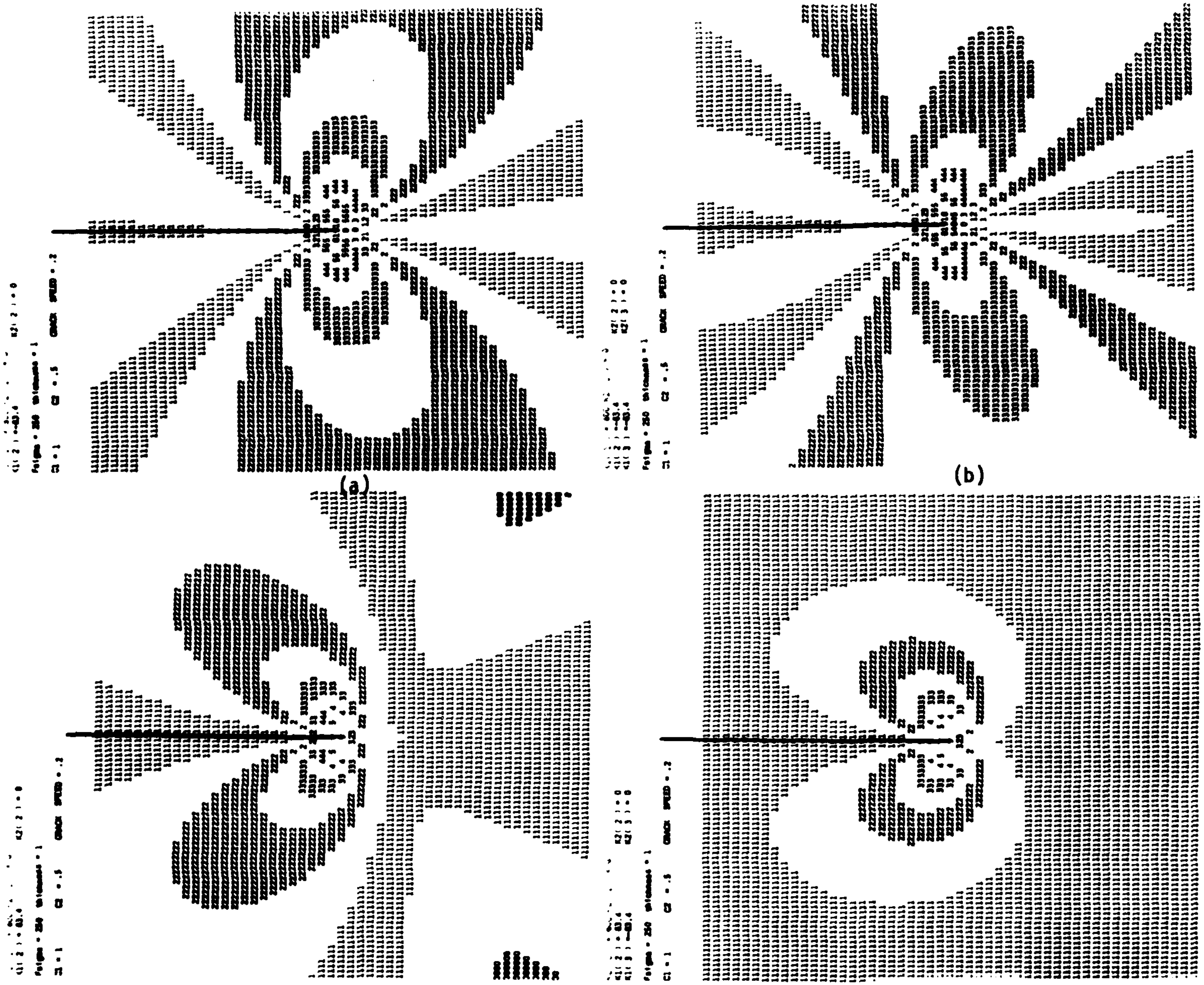

(a) (b) (c) (d)

a) $A_{I2} = -0.58$MPa b) $A_{I2} = -0.58$MPa, $A_{I3} = -0.58$MPa$/\sqrt{m}$
c) $A_{I2} = 0.58$MPa c) $A_{I2} = 0.58$MPa, $A_{I3} = -0.58$MPa$/\sqrt{m}$

Figure 1. Pure Mode I ($K_T = 0.876$MPa$\sqrt{m}$) Isochromatics With Higher Order Terms, $C/C_1 = 0.2$

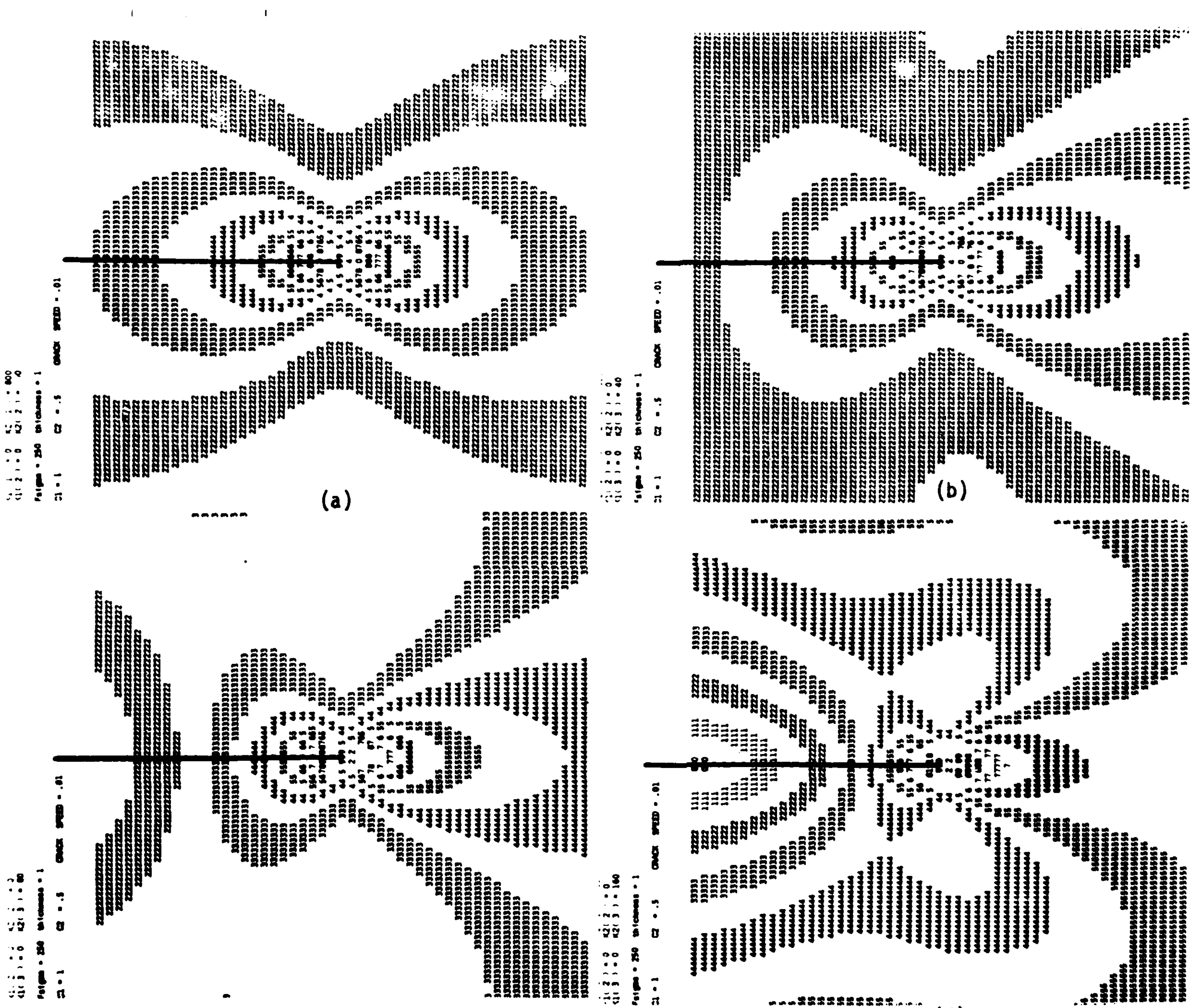

(a) (b) (c) (d)

a) $A_{II3} = 0.0$ b) $A_{II3} = 0.28 MPa/\sqrt{m}$ c) $A_{II3} = 0.55 MPa/\sqrt{m}$ d) $A_{II3} = 1.11 MPa/\sqrt{m}$

Figure 2. Pure Mode II ($K_{II} = 0.876 MPa\sqrt{m}$, $A_{II3} > 0$) Static Isochromatics With Increasing Higher Order Term, A_{II3}

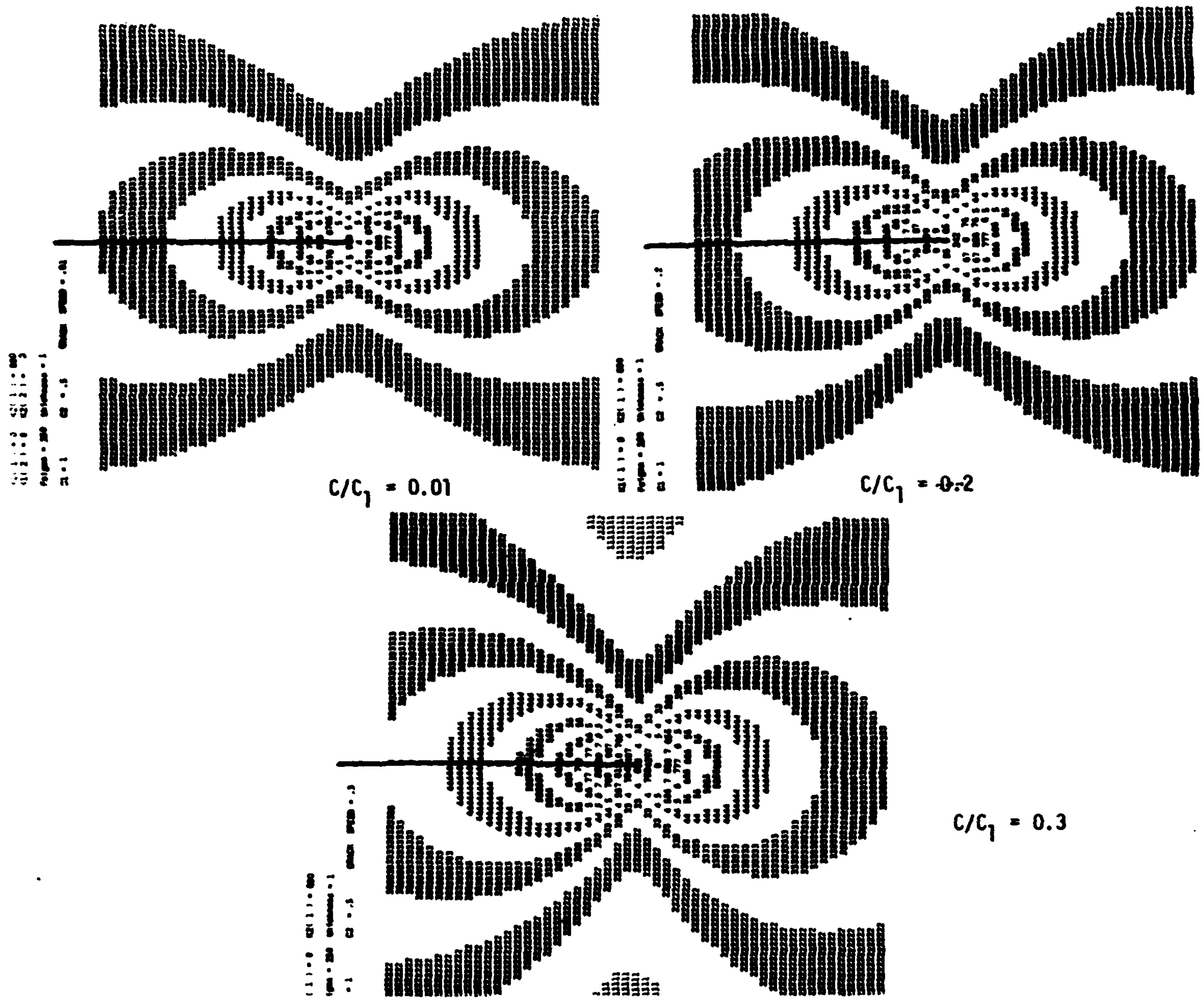

Figure 3. Pure Mode II (K_{II} = 0.876MPa$\sqrt{m}$) Isochromatics

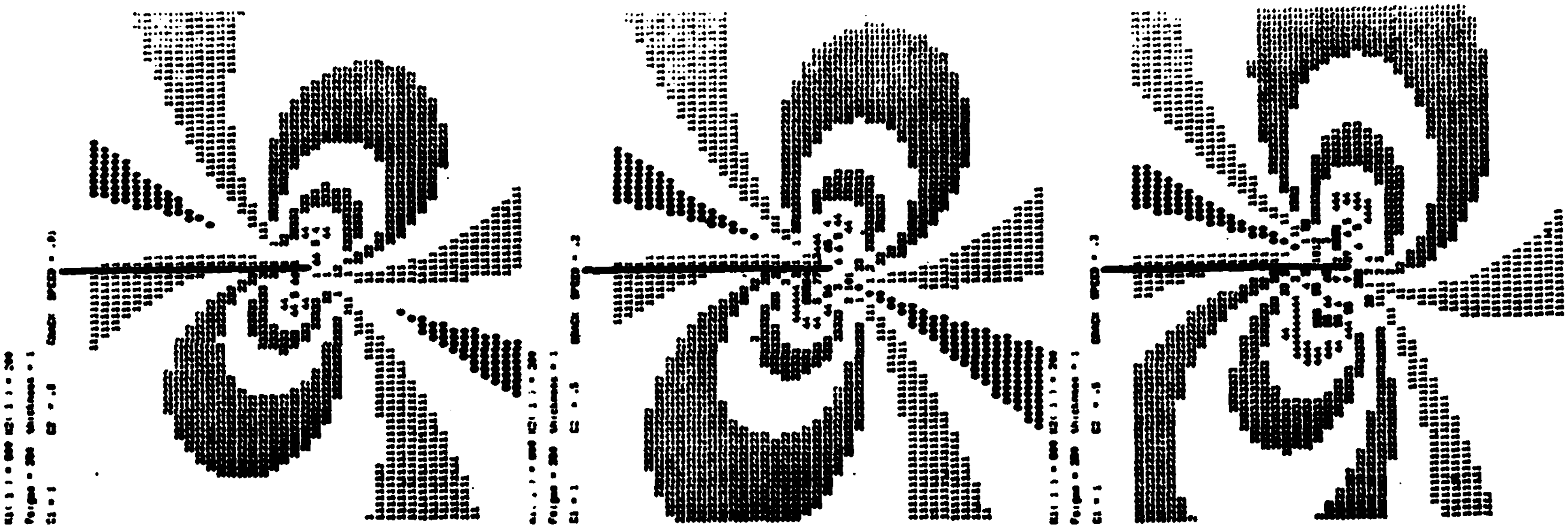

$C/C_1 = 0.01$ $C/C_1 = 0.2$ $C/C_1 = 0.3$

Figure 4. Mixed-mode ($K_{II}/K_I = 0.25$, $K_I = 0.876 MPa\sqrt{m}$) Isochromatics

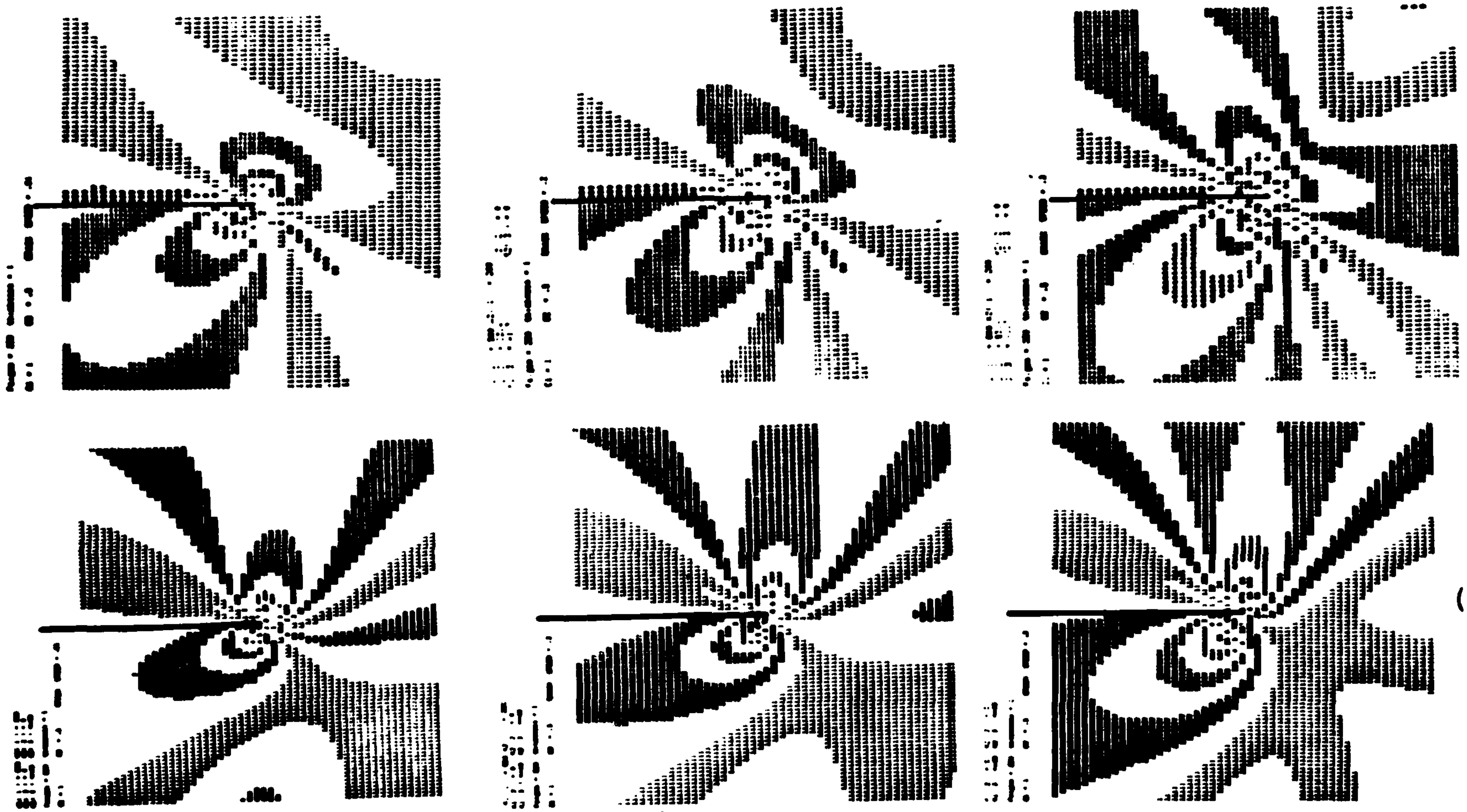

$C/C_1 = 0.01$ $C/C_1 = 0.2$ $C/C_1 = 0.3$

(b)

a) $A_{I2} = 0.58\text{MPa}$, $A_{I3} = 0.29\text{MPa}/\sqrt{m}$ b) $A_{I2} = 0.0$, $A_{I3} = A_{II3} = -0.28\text{MPa}/\sqrt{m}$

Figure 5. Mixed-mode ($K_{II}/K_I = 0.25$, $K_I = 0.876\text{MPa}\sqrt{m}$) Isochromatics. Mode I Dominant Loading With Higher Order Terms of Mode I and Mode II

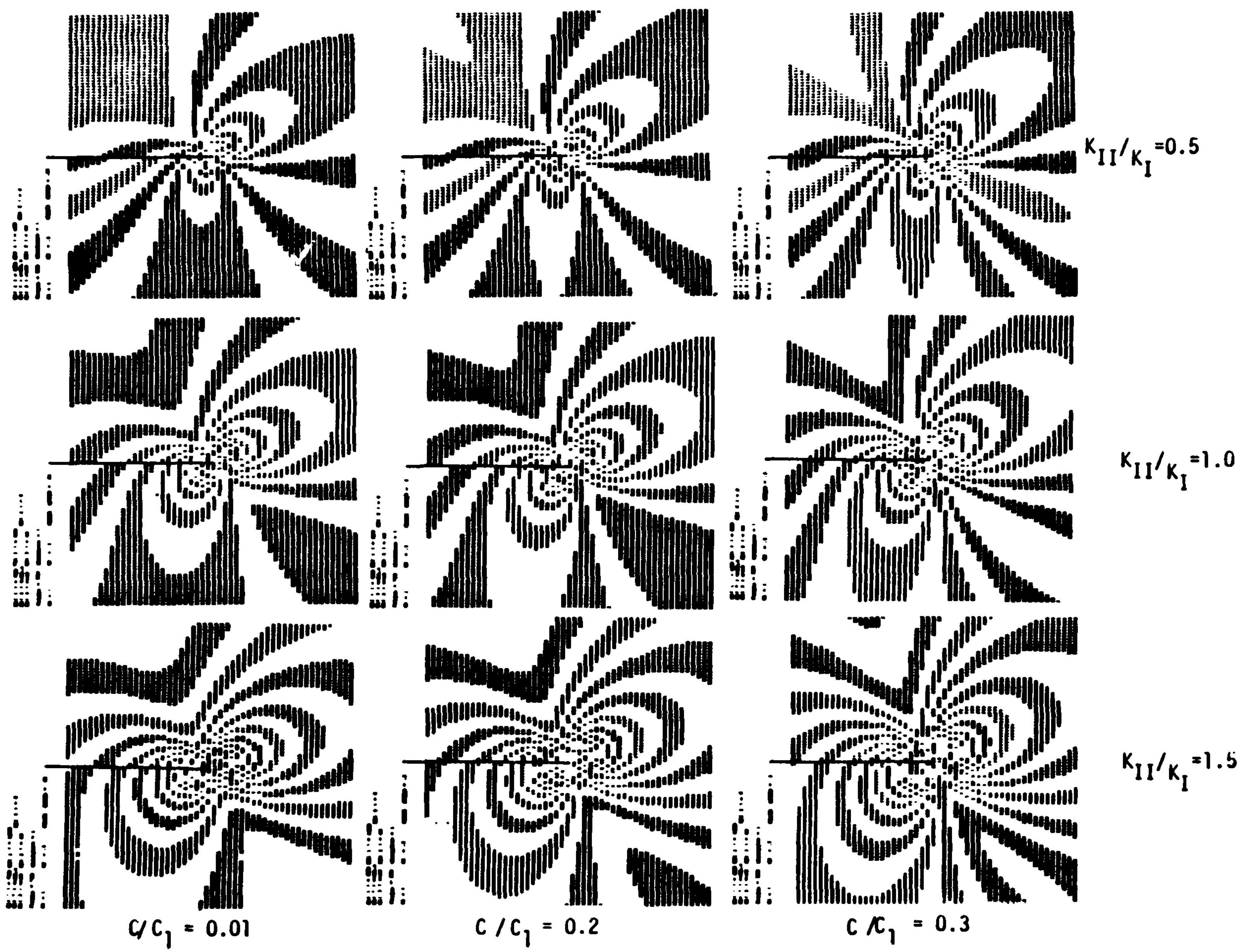

Figure 6. Mixed-mode ($K_I = 0.876 MPa\sqrt{m}$, $A_{I2} = -0.58 MPa$, $A_{I3} = -A_{II3} = -0.28 MPa/\sqrt{m}$) Isochromatics. Mode II Dominant Loading

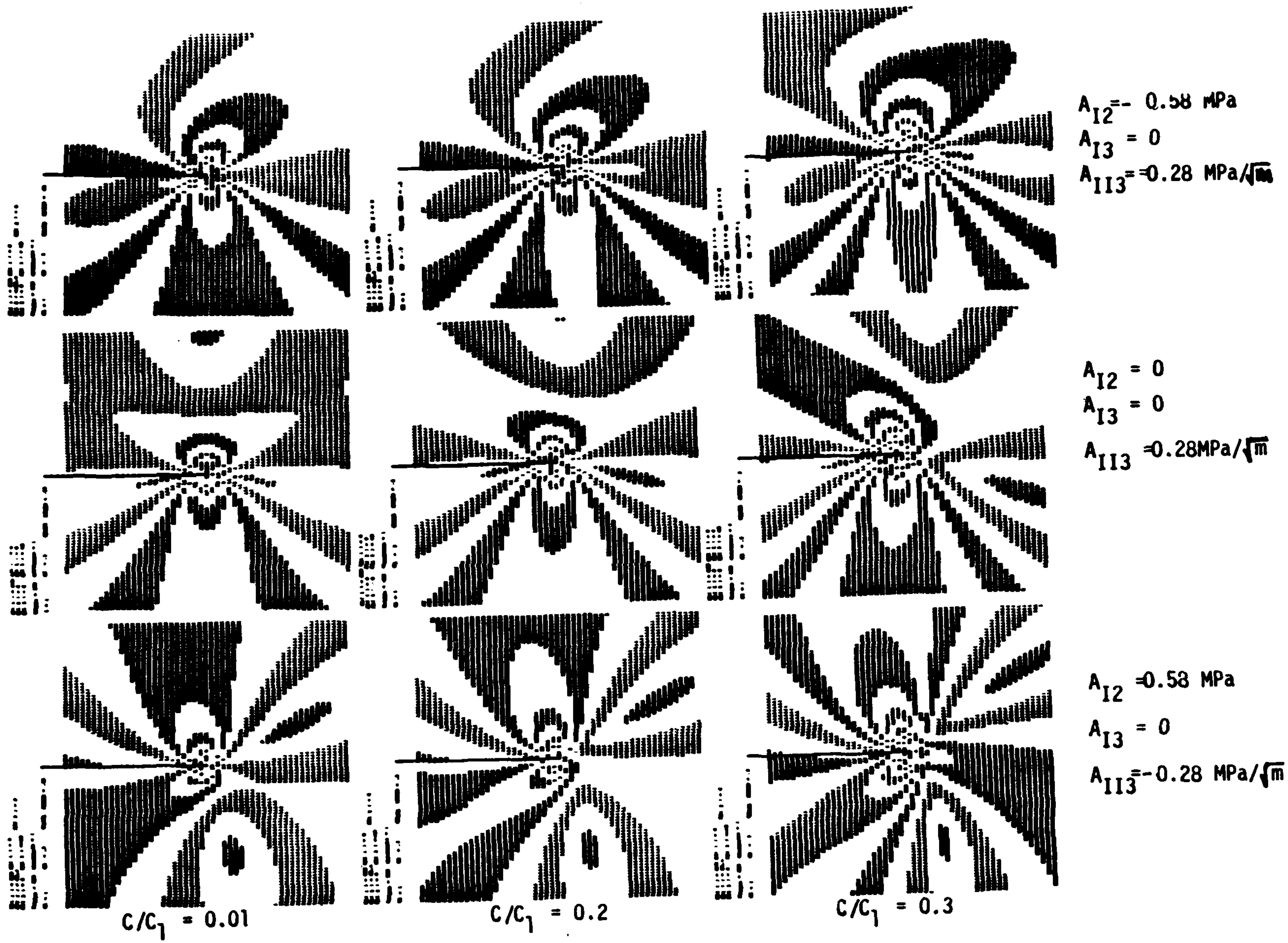

Figure 7. Unsymmetric Isochromatics. Mode I ($K_I = 0.876$MPa$\sqrt{m}$) Dominant Loading, Mode II Higher Order Terms and Increasing Crack Velocity

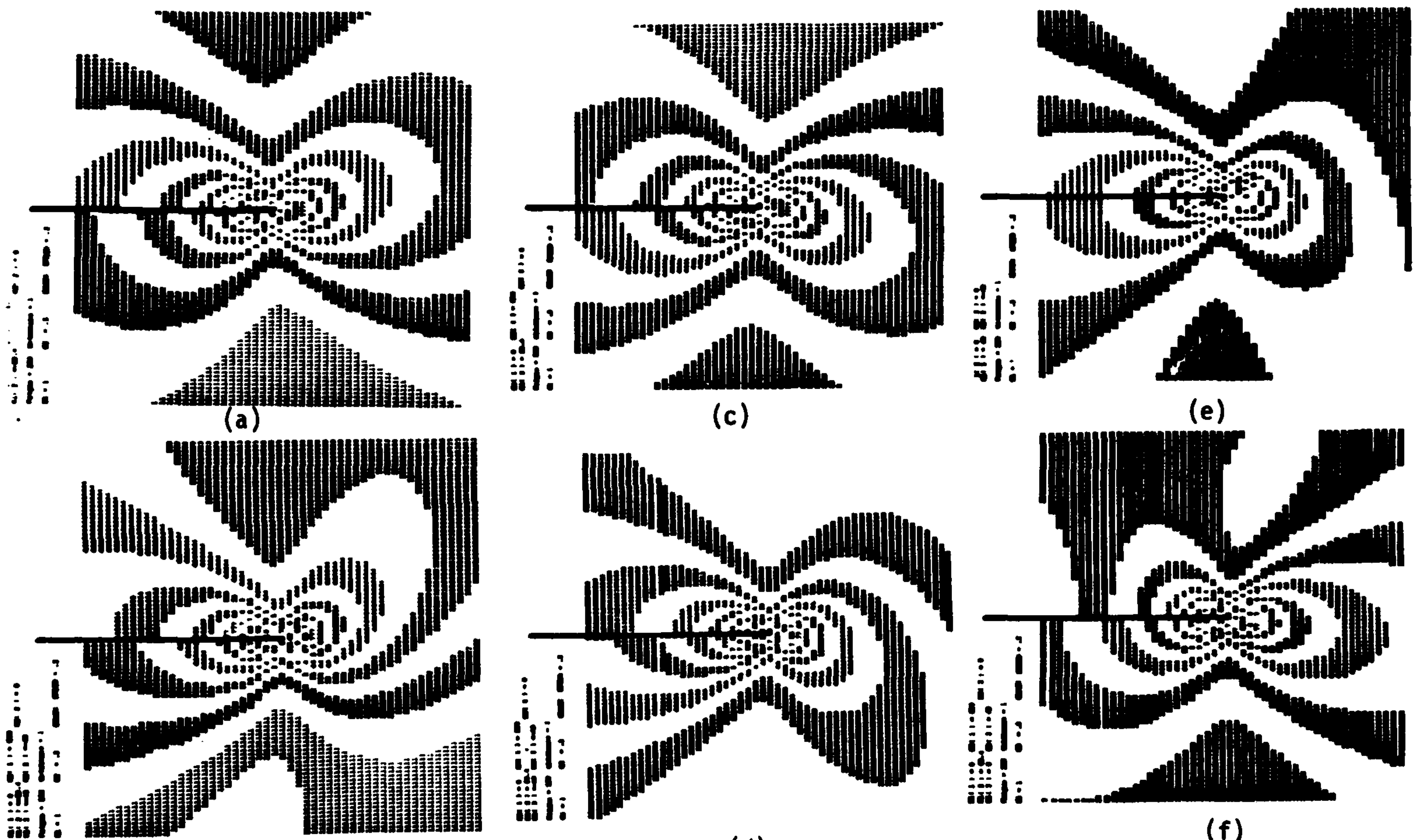

(a) (c) (e)

(b) (d) (f)

a) $A_{I2} = -0.58$ MPa

b) $A_{I2} = -0.58$ MPa
$A_{I3} = A_{II3} = -0.28 \mathrm{MPa}/\sqrt{m}$

c) $A_{I2} = 0.58$ MPa

d) $A_{I2} = 0.58$ MPa
$A_{I3} = A_{II3} = -0.28 \mathrm{MPa}/\sqrt{m}$

e) $A_{I2} = A_{I3} = 0$
$A_{II3} = -0.28 \mathrm{MPa}/\sqrt{m}$

f) $A_{I2} = 0.58 \mathrm{MPa}, A_{I3} = 0$
$A_{II3} = 0.28 \mathrm{MPa}/\sqrt{m}$

Figure 8. Unsymmetric Isochromatics. Mode II ($K_{II} = 0.876 \mathrm{MPa}\sqrt{m}$) Dominant Loading, Mode I Higher Order Terms and Crack Velocity $C/C_1 = 0.2$

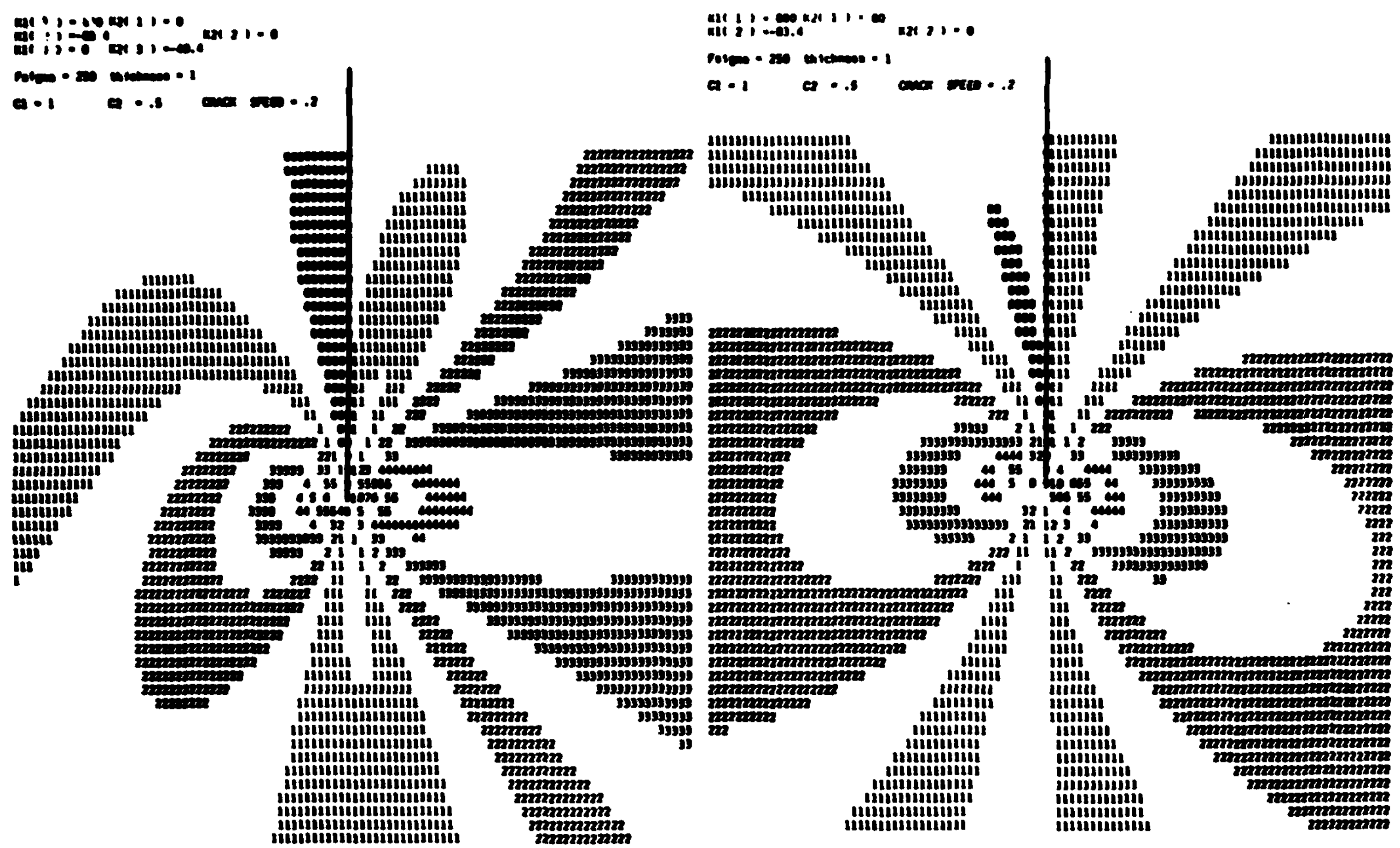

(a) (b)

a) A_{I2} = -0.58MPa, A_{II3} = -0.28MPa/$\sqrt{m}$ b) K_{II}/K_I = 0.10, A_{I2} = -0.58MPa

Figure 9. Unsymmetric Isochromatics, Mode I (K_I = 0.876MPa$\sqrt{m}$) Dominant and Mixed-mode Stresses

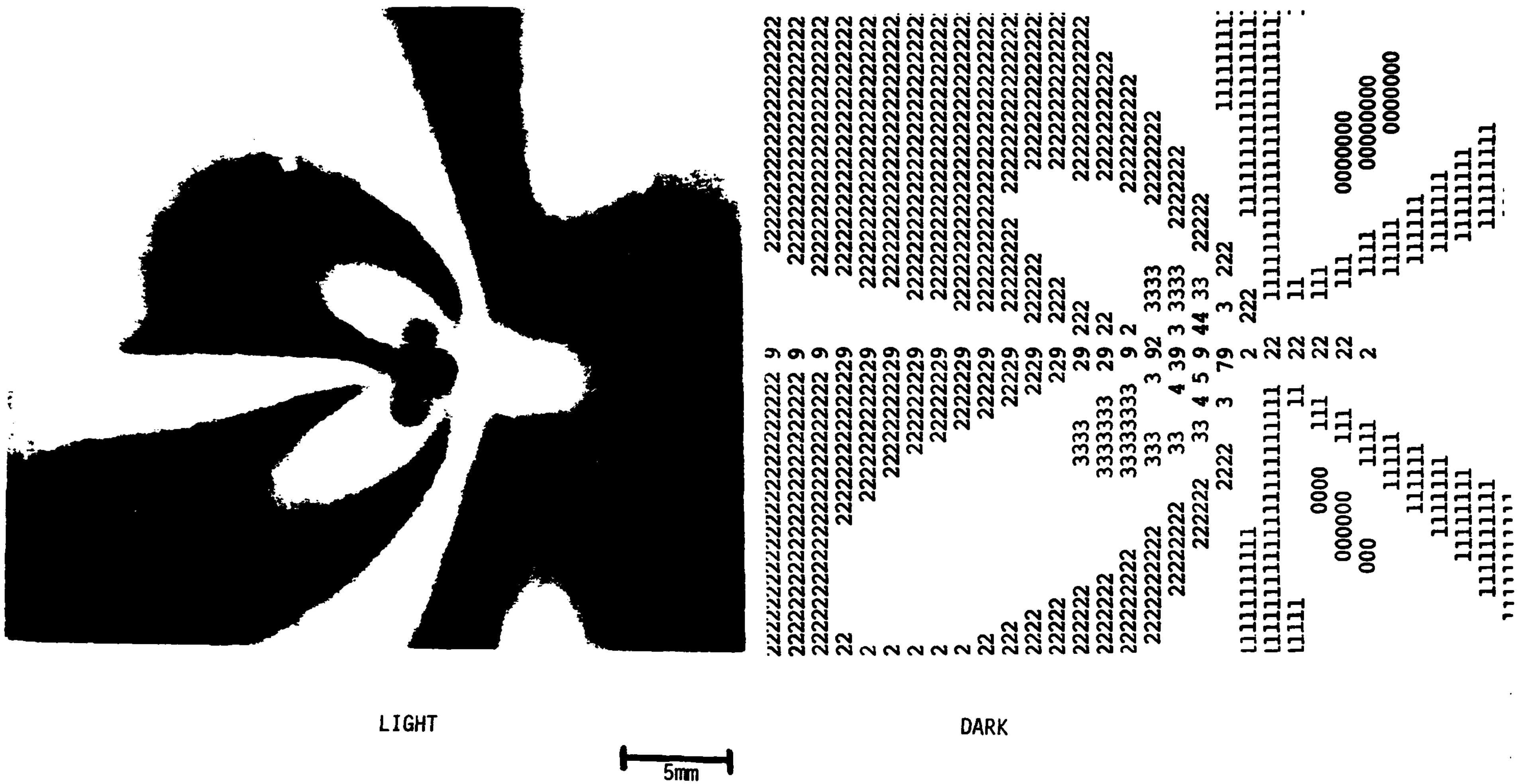

Figure 10. Experimentally and Theoretically Generated Isochromatics Associated With a Curved Crack in Single-Edged-Notch(SEN) Specimen Under Fixed Grip Loading

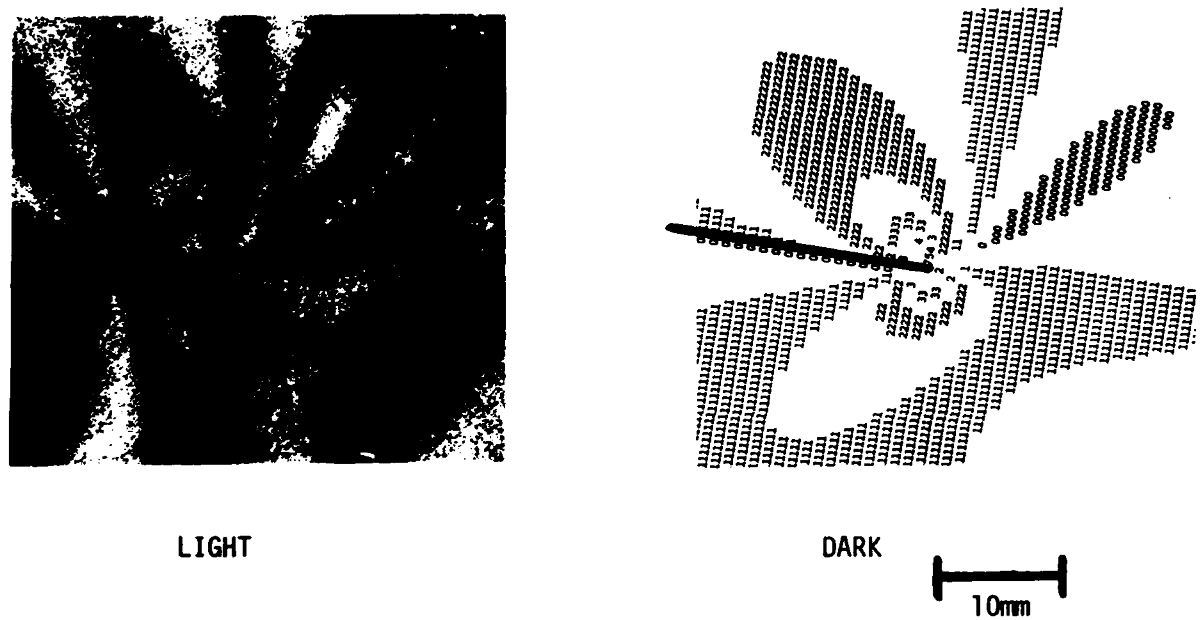

Figure 11. Experimentally and Theoretically Generated Isochromatics Associated With a Curving Post-branched Crack in a Wedge-Loaded Rectangular Double Cantelever Beam (WL-RDCB) Specimen.

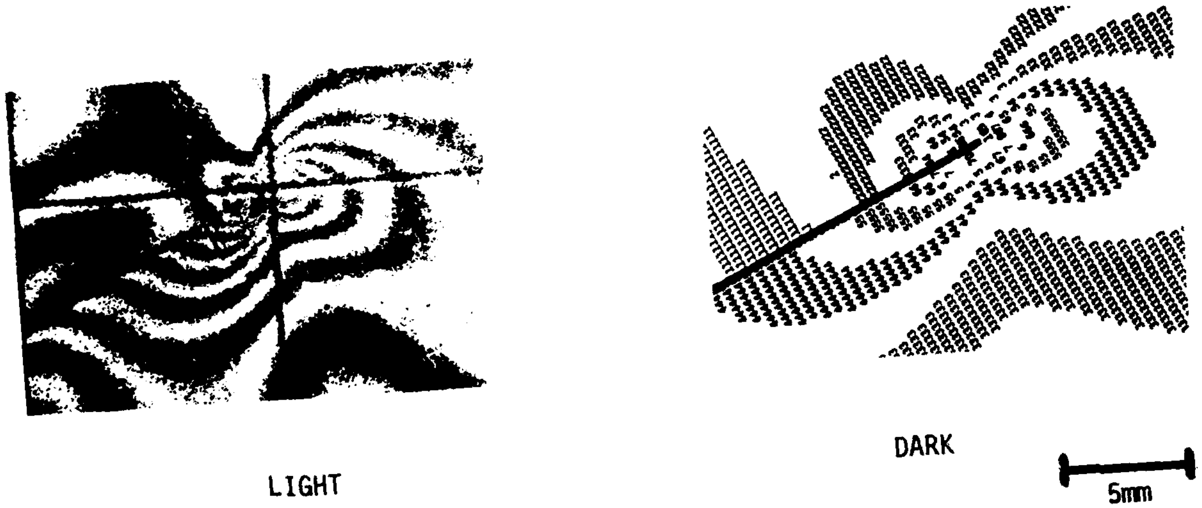

Figure 12. Expeimentally and Theoretically Generated Isochromatics Associated With an Arrested, Branched Crack in a Single-Edged-Notch(SEN) Specimen Under Tension Loading

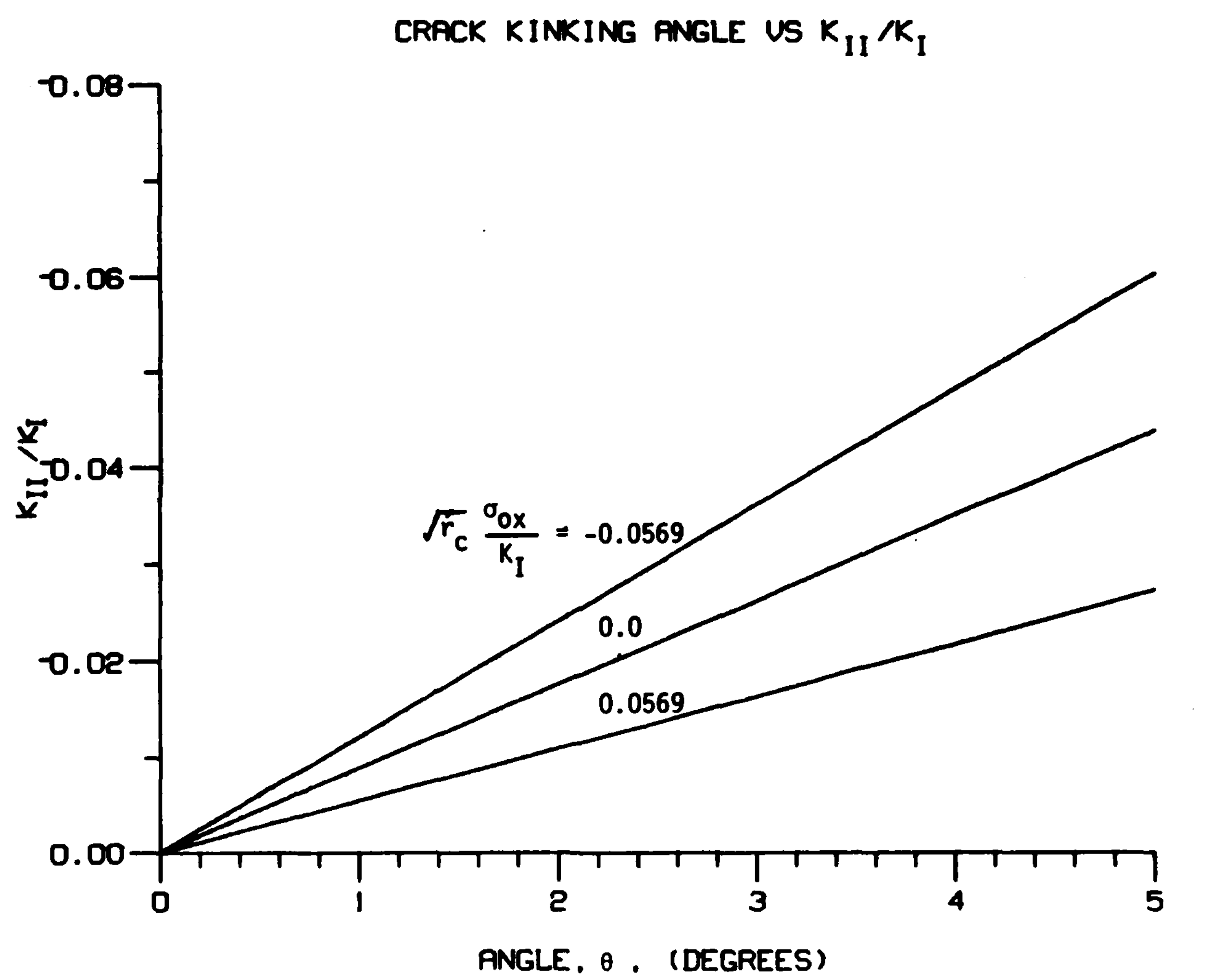

Figure 13. Crack Kinking Angles Associated With Mode I Dominant Loading

Part 1 - Government Administrative and Liaison Activities

Office of Naval Research
Department of the Navy
Arlington, VA 22217
Attn: Code 474 (2)
471
200

Director
Office of Naval Research
Branch Office
666 Summer Street
Boston, MA 02210

Director
Office of Naval Research
Branch Office
536 South Clark Street
Chicago, IL 60605

Director
Office of Naval Research
Branch Office
1030 East Green Street
Pasadena, CA 91106

Naval Research Laboratory (6)
Code 2627
Washington, D.C. 20375

Defense Documentation Center (12)
Cameron Station
Alexandria, Virginia 22314

Navy

Undersea Explosion Research Division
Naval Ship Research and Development
Center
Norfolk Naval Shipyard
Portsmouth, VA 23709
Attn: Dr. E. Palmer, Code 177

Navy (Con't.)

Naval Research Laboratory
Washington, D.C. 20375
Attn: Code 8400
8410
8430
8440
6300
6390
6380

David W. Taylor Naval Ship Research
and Development Center
Annapolis, MD 21402
Attn: Code 2740
28
281

Naval Weapons Center
China Lake, CA 93555
Attn: Code 4062
4520

Commanding Officer
Naval Civil Engineering Laboratory
Code L31
Port Hueneme, CA 93041

Naval Surface Weapons Center
White Oak
Silver Spring, MD 20910
Attn: Code R-10
G-402
K-82

Technical Director
Naval Ocean Systems Center
San Diego, CA 92152

Navy Underwater Sound
Reference Division
Naval Research Laboratory
P.O. Box 8337
Orlando, FL 32806

Navy (Con't.)

Chief of Naval Operations
Department of the Navy
Washington, D.C. 20350
Attn: Code OP-098

Strategic Systems Project Office
Department of the Navy
Washington, D.C. 20376
Attn: NSP-200

Naval Air Systems Command
Department of the Navy
Washington, D.C. 20361
Attn: Code 5302 (Aerospace and Structures)
604 (Technical Library)
320B (Structures)

Naval Air Development Center
Warminster, PA 18974
Attn: Aerospace Mechanics
Code 606

U.S. Naval Academy
Engineering Department
Annapolis, MD 21402

Naval Facilities Engineering Command
200 Stovall Street
Alexandria, VA 22332
Attn.: Code 03 (Research & Development)
04B
045
14114 (Technical Library)

Naval Sea Systems Command
Department of the Navy
Washington, D.C. 20362
Attn: Code 05H
312
322
323
05R
32R

Navy (Con't.)

Commander and Director
David W. Taylor Naval Ship
Research and Development Center
Bethesda, MD 20084
Attn: Code 042
17
172
173
174
1800
1844
012.2
1900
1901
1945
1960
1962

Naval Underwater Systems Center
Newport, RI 02840
Attn: Dr. R. Trainor

Naval Surface Weapons Center
Dahlgren Laboratory
Dahlgren, VA 22448
Attn: Code G04
G20

Technical Director
Mare Island Naval Shipyard
Vallejo, CA 94592

U.S. Naval Postgraduate School
Library
Code 0384
Monterey, CA 93940

Webb Institute of Naval Architecture
Attn: Librarian
Crescent Beach Road, Glen Cove
Long Island, NY 11542

Army

Commanding Officer (2)
U.S. Army Research Office
P.O. Box 12211
Research Triangle Park, NC 27709
Attn: Mr. J. J. Murray, CRD-AA-IP

Army (Con't.)

Watervliet Arsenal
MAGGS Research Center
Watervliet, NY 12189
Attn: Director of Research

U.S. Army Materials and Mechanics
Research Center
Watertown, MA 02172
Attn: Dr. R. Shea, DRXMR-T

U.S. Army Missile Research and
Development Center
Redstone Scientific Information
Center
Chief, Document Section
Redstone Arsenal, AL 35809

Army Research and Development
Center
Fort Belvoir, VA 22060

NASA

National Aeronautics and Space
Administration
Structures Research Division
Langley Research Center
Langley Station
Hampton, VA 23365

National Aeronautics and Space
Administration
Associate Administrator for Advanced
Washington, D.C. 20546

Air Force

Wright-Patterson Air Force Base
Dayton, OH 45433
Attn: AFFDL (FB)
(FBR)
(FBE)
(FBS)
AFML (MBM)

Air Force (Con't.)

Chief Applied Mechanics Group
U.S. Air Force Institute of Technology
Wright-Patterson Air Force Base
Dayton, OH 45433

Chief, Civil Engineering Branch
WLRC, Research Division
Air Force Weapons Laboratory
Kirtland Air Force Base
Albuquerque, NM 87117

Air Force Office of Scientific Research
Bolling Air Force Base
Washington, D.C. 20332
Attn: Mechanics Division

Department of the Air Force
Air University Library
Maxwell Air Force Base
Montgomery, AL 36112

Other Government Activities

Commandant
Chief, Testing and Development Division
U.S. Coast Guard
1300 E Street, NW.
Washington, D.C. 20226

Technical Director
Marine Corps Development
and Education Command
Quantico, VA 22134

Director Defense Research
and Engineering
Technical Library
Room 3C128
The Pentagon
Washington, D.C. 20301

Other Government Activities (Con't.)

Dr. M. Gaus
National Science Foundation
Environmental Research Division
Washington, D.C. 20550

Library of Congress
Science and Technology Division
Washington, D.C. 20540

Director
Defense Nuclear Agency
Washington, D.C. 20305
Attn: SPSS

Mr. Jerome Persh
Staff Specialist for Materials
and Structures
OUSDR&E, The Pentagon
Room 3D1089
Washington, D.C. 20301

Chief, Airframe and Equipment Branch
FS-120
Office of Flight Standards
Federal Aviation Agency
Washington, D.C. 20553

National Academy of Sciences
National Research Council
Ship Hull Research Committee
2101 Constitution Avenue
Washington, D.C. 20418
Attn: Mr. A. R. Lytle

National Science Foundation
Engineering Mechanics Section
Division of Engineering
Washington, D.C. 20550

Picatinny Arsenal
Plastics Technical Evaluation Center
Attn: Technical Information Section
Dover, NJ 07810

Maritime Administration
Office of Maritime Technology
14th and Constitution Ave., NW.
Washington, D.C. 20230

PART 2 - Contractors and Other Technical Collaborators

Universities

Dr. J. Tinsley Oden
University of Texas at Austin
345 Engineering Science Building
Austin, TX 78712

Professor Julius Miklowitz
California Institute of Technology
Division of Engineering
and Applied Sciences
Pasadena, CA 91109

Dr. Harold Liebowitz, Dean
School of Engineering and
Applied Science
George Washington University
Washington, D.C. 20052

Professor Eli Sternberg
California Institute of Technology
Division of Engineering and
Applied Sciences
Pasadena, CA 91109

Professor Paul M. Naghdi
University of California
Department of Mechanical Engineering
Berkeley, CA 94720

Professor A. J. Durelli
Oakland University
School of Engineering
Rochester, MO 48063

Professor F. L. DiMaggio
Columbia University
Department of Civil Engineering
New York, NY 10027

Professor Norman Jones
The University of Liverpool
Department of Mechanical Engineering
P.O. Box 147
Brownlow Hill
Liverpool L69 3BX
England

Professor E. J. Skudrzyk
Pennsylvania State University
Applied Research Laboratory
Department of Physics
State College, PA 16801

Universities (Con't.)

Professor J. Klosner
Polytechnic Institute of New York
Department of Mechanical and
Aerospace Engineering
333 Jay Street
Brooklyn, NY 11201

Prof. R. A. Schapery
Texas A&M University
Department of Civil Engineering
College Station, TX 77843

Professor Walter D. Pilkey
University of Virginia
Research Laboratories for the
Engineering Sciences and
Applied Sciences
Charlottesville, VA 22901

Professor K. D. Willmert
Clarkson College of Technology
Department of Mechanical Engineering
Potsdam, NY 13676

Dr. Walter E. Haisler
Texas A&M University
Aerospace Engineering Department
College Station, TX 77843

Dr. Hussein A. Kamel
University of Arizona
Department of Aerospace and
Mechanical Engineering
Tucson, AZ 85721

Dr. S. J. Fenves
Carnegie-Mellon University
Department of Civil Engineering
Schenley Park
Pittsburgh, PA 15213

Dr. Ronald L. Huston
Department of Engineering Analysis
University of Cincinnati
Cincinnati, OH 45221

Universities (Con't.)

Professor G. C. M. Sih
Lehigh University
Institute of Fracture and
Solid Mechanics
Bethlehem, PA 18015

Professor Albert S. Kobayashi
University of Washington
Department of Mechanical Engineering
Seattle, WA 98105

Professor Daniel Frederick
Virginia Polytechnic Institute and
State University
Department of Engineering Mechanics
Blacksburg, VA 24061

Professor A. C. Eringen
Princeton University
Department of Aerospace and
Mechanical Sciences
Princeton, NJ 08540

Professor E. H. Lee
Stanford University
Division of Engineering Mechanics
Stanford, CA 94305

Professor Albert I. King
Wayne State University
Biomechanics Research Center
Detroit, MI 48202

Dr. V. R. Hodgson
Wayne State University
School of Medicine
Detroit, MI 48202

Dean B. A. Boley
Northwestern University
Department of Civil Engineering
Evanston, IL 60201

Universities (Con't.)

Professor P. G. Hodge, Jr.
University of Minnesota
Department of Aerospace Engineering
and Mechanics
Minneapolis, MN 55455

Dr. D. C. Drucker
University of Illinois
Dean of Engineering
Urbana, IL 61801

Professor N. J. Newmark
University of Illinois
Department of Civil Engineering
Urbana, IL 61803

Professor E. Reissner
University of California, San Diego
Department of Applied Mechanics
La Jolla, CA 92037

Professor William A. Nash
University of Massachusetts
Department of Mechanics and
Aerospace Engineering
Amherst, MA 01002

Professor G. Herrmann
Stanford University
Department of Applied Mechanics
Stanford, CA 94305

Professor J. D. Achenbach
Northwest University
Department of Civil Engineering
Evanston, IL 60201

Professor S. B. Dong
University of California
Department of Mechanics
Los Angeles, CA 90024

Professor Burt Paul
University of Pennsylvania
Towne School of Civil and
Mechanical Engineering
Philadelphia, PA 19104

Universities (Con't.)

Professor H. W. Liu
Syracuse University
Department of Chemical Engineering
and Metallurgy
Syracuse, NY 13210

Professor S. Bodner
Technion R&D Foundation
Haifa, Israel

Professor Werner Goldsmith
University of California
Department of Mechanical Engineering
Berkeley, CA 94720

Professor R. S. Rivlin
Lehigh University
Center for Application
of Mathematics
Bethlehem, PA 18015

Professor F. A. Cozzarelli
State University of New York at
Buffalo
Division of Interdisciplinary Studies
Karr Parker Engineering Building
Chemistry Road
Buffalo, NY 14214

Professor Joseph L. Rose
Drexel University
Department of Mechanical Engineering
and Mechanics
Philadelphia, PA 19104

Professor B. K. Donaldson
University of Maryland
Aerospace Engineering Department
College Park, MD 20742

Professor Joseph A. Clark
Catholic University of America
Department of Mechanical Engineering
Washington, D.C. 20064

Universities (Con't.)

Dr. Samuel B. Batdorf
University of California
School of Engineering
and Applied Science
Los Angeles, CA 90024

Professor Isaac Fried
Boston University
Department of Mathematics
Boston, MA 02215

Professor E. Krempl
Rensselaer Polytechnic Institute
Division of Engineering
Engineering Mechanics
Troy, NY 12181

Dr. Jack R. Vinson
University of Delaware
Department of Mechanical and Aerospace
Engineering and the Center for
Composite Materials
Newark, DE 19711

Dr. J. Duffy
Brown University
Division of Engineering
Providence, RI 02912

Dr. J. L. Swedlow
Carnegie-Mellon University
Department of Mechanical Engineering
Pittsburgh, PA 15213

Dr. V. K. Varadan
Ohio State University Research Foundation
Department of Engineering Mechanics
Columbus, OH 43210

Dr. Z. Hashin
University of Pennsylvania
Department of Metallurgy and
Materials Science
College of Engineering and
Applied Science
Philadelphia, PA 19104

Universities (Con't.)

Dr. Jackson C. S. Yang
University of Maryland
Department of Mechanical Engineering
College Park, MD 20742

Professor T. Y. Chang
University of Akron
Department of Civil Engineering
Akron, OH 44325

Professor Charles W. Bert
University of Oklahoma
School of Aerospace, Mechanical,
and Nuclear Engineering
Norman, OK 73019

Professor Satya N. Atluri
Georgia Institute of Technology
School of Engineering and
Mechanics
Atlanta, GA 30332

Professor Graham F. Carey
University of Texas at Austin
Department of Aerospace Engineering
and Engineering Mechanics
Austin, TX 78712

Dr. S. S. Wang
University of Illinois
Department of Theoretical and
Applied Mechanics
Urbana, IL 61801

Industry and Research Institutes

Dr. Norman Hobbs
Kaman AviDyne
Division of Kaman
Sciences Corporation
Burlington, MA 01803

Argonne National Laboratory
Library Services Department
9700 South Cass Avenue
Argonne, IL 60440

Industry and Research Institutes (Con't.)

Dr. M. C. Junger
Cambridge Acoustical Associates
54 Rindge Avenue Extension
Cambridge, MA 02140

Dr. V. Godino
General Dynamics Corporation
Electric Boat Division
Groton, CT 06340

Dr. J. E. Greenspon
J. G. Engineering Research Associates
3831 Menlo Drive
Baltimore, MD 21215

Newport News Shipbuilding and
Dry Dock Company
Library
Newport News, VA 23601

Dr. W. F. Bozich
McDonnell Douglas Corporation
5301 Bolsa Avenue
Huntington Beach, CA 92647

Dr. H. N. Abramson
Southwest Research Institute
8500 Culebra Road
San Antonio, TX 78284

Dr. R. C. DeHart
Southwest Research Institute
8500 Culebra Road
San Antonio, TX 78284

Dr. M. L. Baron
Weidlinger Associates
110 East 59th Street
New York, NY 10022

Dr. T. L. Geers
Lockheed Missiles and Space Company
3251 Hanover Street
Palo Alto, CA 94304

Mr. William Caywood
Applied Physics Laboratory
Johns Hopkins Road
Laurel, MD 20810

Industry and Research Institutes (Con't.)

Dr. Robert E. Dunham
Pacifica Technology
P.O. Box 148
Del Mar, CA 92014

Dr. M. F. Kanninen
Battelle Columbus Laboratories
505 King Avenue
Columbus, OH 43201

Dr. A. A. Hochrein
Daedalean Associates, Inc.
Springlake Research Road
15110 Frederick Road
Woodbine,, MD 21797

Dr. James W. Jones
Swanson Service Corporation
P.O. Box 5415
Huntington Beach, CA 92646

Dr. Robert E. Nickell
Applied Science and Technology
3344 North Torrey Pines Court
Suite 220
La Jolla, CA 92037

Dr. Kevin Thomas
Westinghouse Electric Corp.
Advanced Reactors Division
P.O. Box 158
Madison, PA 15663

Dr. Bernard Shaffer
Polytechnic Institute of New York
Dept. of Mechanical and Aerospace
Engineering
333 Jay Street
Brooklyn,, NY 11021

UNCLASSIFIED

SECURITY CLASSIFICATION OF THIS PAGE (When Data Entered)

REPORT DOCUMENTATION PAGE

READ INSTRUCTIONS BEFORE COMPLETING FORM

1. REPORT NUMBER UWA/DME/TR-84/49	2. GOVT ACCESSION NO. AD-A143 329	3. RECIPIENT'S CATALOG NUMBER
4. TITLE (and Subtitle) Analysis of dynamic mixed mode crack tip stress patterns.		5. TYPE OF REPORT & PERIOD COVERED Technical Report
		6. PERFORMING ORG. REPORT NUMBER UWA/DME/TR-84/49
7. AUTHOR(s) M. Ramulu, D. B. Barker, and A. S. Kobayashi		8. CONTRACT OR GRANT NUMBER(s) N00014-76-C-0060
9. PERFORMING ORGANIZATION NAME AND ADDRESS Dept. of Mechanical Engineering, FU-10 University of Washington Seattle, Washington 98195		10. PROGRAM ELEMENT, PROJECT, TASK AREA & WORK UNIT NUMBERS NR 064-478
11. CONTROLLING OFFICE NAME AND ADDRESS Office of Naval Research Arlington, VA 22217		12. REPORT DATE May 1984
		13. NUMBER OF PAGES 31
14. MONITORING AGENCY NAME & ADDRESS (if different from Controlling Office)		15. SECURITY CLASS. (of this report) Unclassified
		15a. DECLASSIFICATION/DOWNGRADING SCHEDULE

16. DISTRIBUTION STATEMENT (of this Report)

Unlimited

17. DISTRIBUTION STATEMENT (of the abstract entered in Block 20, if different from Report)

18. SUPPLEMENTARY NOTES

19. KEY WORDS (Continue on reverse side if necessary and identify by block number)

Dynamic mixed mode stress intensity ~~factors, dynamic~~ photoelasticity, crack curving, crack branching, crack kinking angle, error estimates, higher order terms, asymmetric isochromatics.

20. ABSTRACT (Continue on reverse side if necessary and identify by block number)

The mixed-mode, elasto-dynamic state of stresses in the neighborhood of a rapidly running crack tip has been used to develop a relation between the isochromatic fringe order, N, and its position parameters r and θ. The maximum shear stress is expressed in terms of the stress intensity factors K_I, K_{II}, σ_{ox}, and other higher order terms involving the mixed-mode loading for a crack propagating at constant velocity. A graphics package based on these derivations was developed for mapping the isochromatics in the

DD FORM 1 JAN 73 1473 EDITION OF 1 NOV 65 IS OBSOLETE

S/N 0102-014-6601

UNCLASSIFIED

SECURITY CLASSIFICATION OF THIS PAGE (When Data Entered)

20. ABSTRACT

vicinity of a running crack tip and was used to illustrate typical mixed-mode isochromatics. The unsymmetry associated with higher order terms of mixed-mode stress field with the mode I singular stress field and with/without the mode II singular stress field also is investigated. Error estimates due to the assumed presence of K_{II} in a K_I stress field was found to be significant when the distance from the crack tip is more than 4mm.

END

FILMED

8-84

DTIC